Available online at www.eccomasproceedia.org
Eccomas Proceedia COMPDYN (2025) 22- 4

ECCOMAS Proceedia

COMPDYN 2025
10th ECCOMAS Thematic Conference on
Computational Methods in Structural Dynamics and Earthquake Engineering
M. Papadrakakis, M. Fragiadakis (eds.)
Rhodes Island, Greece, 15-18 June 2025

APPLICATION OF THE EXTENDED MODIFIED BRIDGE SYSTEM (EMBS) METHOD IN SEISMIC VEHICLE-BRIDGE INTERACTION

Hossein Homaei[1, 2], Pedro A. Montenegro[3], Charikleia D. Stoura[4], Elias G. Dimitrakopoulos[1]

[1] Department of Civil and Environmental Engineering, Hong Kong University of Science and Technology, Clear Water Bay, Kowloon, Hong Kong, China
hhomaei@connect.ust.hk, ilias@ust.hk

[2]Department of Civil Engineering, Sharif University of Technology, Tehran, Iran

[3] CONSTRUCT - LESE, Faculty of Engineering, Rua Dr. Roberto Frias s/n, 4200-465, University of Porto, Porto, Portugal
paires@fe.up.pt

[4] Institute of Structural Engineering, Department of Civil, Environmental and Geomatic Engineering, ETH, Zurich, Switzerland
charikleia.stoura@ibk.baug.ethz.ch

Abstract

Seismic vehicle-bridge interaction (SVBI) refers to the analysis of vehicle-bridge interaction (VBI) under the effect of earthquake excitation. SVBI evaluates the seismic performance of the entire vehicle-bridge system, necessitating the development of sophisticated coupled vehicle-bridge models. The Extended Modified Bridge System (EMBS) method is a consistent approach for decoupling the SVBI problem, bypassing the challenges associated with the analysis of a coupled VBI system. The EMBS method splits the equation of motion (EOM) of the bridge into zero-order and first-order EOMs through an asymptotic expansion analysis, allowing an independent analysis of the bridge subsystem without explicitly modeling the interaction between the vehicle and bridge subsystems. Subsequently, it solves the EOM of the vehicle subsystem by using the bridge response as an input. The EMBS method was initially proposed analytically and demonstrated numerically for a simply supported bridge. The current study demonstrates the feasibility of applying the EMBS method to a complex railway bridge, taking into account the track and substructure.

Keywords: Seismic Vehicle-Bridge Interaction, Decoupled Approach, Extended Modified Bridge System (EMBS) Method, Railway Bridges

doi: 10.7712/120125.12655.24450

1 INTRODUCTION

High-speed railway (HSR) lines feature significantly more bridges than conventional railway lines [1]. In some instances, bridges make up over 90% of the total length of an HSR line. For example, on the Guangzhou-Zhuhai line in China, bridges account for 94.2% of its total length of 142.3 km [2]. As the number of bridges in HSR lines increases and HSR networks expand into seismic-prone areas [3, 4], the likelihood of a seismic event occurring while a train traverses a bridge rises significantly. This underscores the importance of studying the effect of vehicle-bridge interaction (VBI) during earthquake excitation, particularly concerning the seismic response of both bridges (see [5-8]) and trains (see [9, 10]).

Seismic vehicle-bridge interaction (SVBI) refers to the analysis of VBI under earthquake excitation, focusing on the seismic performance of the entire vehicle-bridge system. This requires the development of an elaborate coupled vehicle-bridge model. Several studies [11-15] developed robust and high-fidelity simulation schemes for SVBI. For example, Li et al. [16, 17] introduced a numerical model for a three-dimensional train-wheel-bridge-bearing system subjected to seismic events. However, developing such a complex coupled SVBI model presents significant challenges, primarily due to the lack of Finite Element Method (FEM) software that is suitable for civil engineering applications and capable of accurately modeling a coupled VBI system during earthquake excitation [18].

To bypass the challenges associated with the analysis of coupled VBI systems subjected to earthquake excitation, several studies attempted to decouple the vehicle-bridge system [19-21]. In this context, Homaei et al. [22] introduced the Extended Modified Bridge System (EMBS) method, originally established for VBI systems without the effect of earthquake [23], for decoupling the SVBI problem. The EMBS method accommodates multi-degree of freedom (MDOF) models for both vehicles and bridges, effectively capturing the dynamics of complex SVBI systems. That study [22] focused on the theoretical derivation of the EMBS formulation and demonstrated the accuracy of the proposed EMBS approach solely on a simply supported bridge.

The current study demonstrates the applicability of the EMBS method in analyzing a complex railway bridge traversed by a practical train, additionally incorporating the track and substructure of the bridge. Specifically, it considers the case of Alverca viaduct [24] under the passage of the Siemens Velaro AVE-S103 train [25] during a seismic event, as demonstrated in the study of Montenegro et al. [24]. This study compares the response of the bridge and the train, considering two approaches: the coupled method presented in the study of Montenegro et al. [24] and the uncoupled EMBS method presented by Homaei et al. [22].

2 FORMULATION OF THE SEISMIC VEHICLE-BRIDGE INTERACTION

This section outlines the formulation of the EMBS method for decoupling MDOF vehicle-bridge systems under earthquake excitation [22]. The equation of motion (EOM) of a coupled VBI system can be written as [26]:

$$\mathbf{m}\ddot{\tilde{\mathbf{u}}}+\mathbf{c}\dot{\tilde{\mathbf{u}}}+\mathbf{k}\tilde{\mathbf{u}}-\tilde{\mathbf{W}}\tilde{\boldsymbol{\lambda}}=\mathbf{f} \tag{1}$$

where $\mathbf{m}$ represents the mass matrix, $\mathbf{c}$ indicates the damping matrix, $\mathbf{k}$ denotes the stiffness matrix, $\tilde{\mathbf{u}}(t)$ indicates the displacement vector, $\tilde{\mathbf{W}}$ represents the contact direction matrix, $\tilde{\boldsymbol{\lambda}}$ is the contact force vector, and $\mathbf{f}$ represents the external force vector acting on the coupled vehicle-bridge system. Throughout this study, the tilde distinguishes dimensional from the corresponding dimensionless quantities when needed (later on), and an overdot indicates differentiation with respect to the (dimensional) time t. We can state the displacement vector of the whole (coupled) system $\tilde{\mathbf{u}}(t)$ as:

$$\tilde{\mathbf{u}}^{\mathrm{T}} = \begin{bmatrix} \tilde{\mathbf{u}}_V^{\mathrm{T}} & \tilde{\mathbf{u}}_B^{\mathrm{T}} \end{bmatrix} = \begin{bmatrix} \begin{bmatrix} \tilde{\mathbf{u}}_u^{\mathrm{T}} & \tilde{\mathbf{u}}_w^{\mathrm{T}} \end{bmatrix} & \tilde{\mathbf{u}}_B^{\mathrm{T}} \end{bmatrix} \tag{2}$$

in which (and throughout this study), superscript $()^{\mathrm{T}}$ denotes the transpose of a vector or matrix, subscript $()_V$ represents the vehicle subsystem, and subscript $()_B$ indicates the bridge subsystem.

We consider the EOM of the vehicle about its statically deformed configuration under its self-weight. Accordingly, the EOM of the upper part of the vehicle, which emanates from Equation (1) (see [22] for further details), takes the form:

$$\begin{aligned} &\mathbf{m}_u \ddot{\tilde{\mathbf{u}}}_u + \mathbf{c}_u \dot{\tilde{\mathbf{u}}}_u + \mathbf{k}_u \tilde{\mathbf{u}}_u = \\ &-\mathbf{m}_u \boldsymbol{\delta}_u \ddot{\tilde{u}}_g - \mathbf{c}_{u,w} \tilde{\mathbf{W}}_w^{-\mathrm{T}} \left(v \tilde{\mathbf{W}}_B'^{\mathrm{T}} \tilde{\mathbf{u}}_B + \tilde{\mathbf{W}}_B^{\mathrm{T}} \dot{\tilde{\mathbf{u}}}_B + v \mathbf{r}_c' \right) - \mathbf{k}_{u,w} \tilde{\mathbf{W}}_w^{-\mathrm{T}} \left(\tilde{\mathbf{W}}_B^{\mathrm{T}} \tilde{\mathbf{u}}_B + \mathbf{r}_c \right) \end{aligned} \tag{3}$$

where $\ddot{\tilde{u}}_g$ represents the ground acceleration at the base of the bridge, and $\boldsymbol{\delta}$ is a unit vector connecting the ground motion to the pertinent degrees of freedom (DOFs). Throughout this study, subscript $()_u$ indicates the upper part of the vehicle, subscript $()_w$ denotes the wheels part, and subscript $()_{u,w}$ represents the coupling terms between the upper and wheels parts of the vehicle. Section 3.2, later on, clarifies the modeling assumptions for the vehicle. $\tilde{\mathbf{W}}_B(x)$ is the contact direction matrix of the bridge connecting the contact forces between the two systems with the DOFs of the bridge. $\tilde{\mathbf{W}}_B(x)$ is time-dependent [26] as the location of the vehicle $x = vt$ changes with time t (v indicates the vehicle speed). Similarly, $\tilde{\mathbf{W}}_w$ associates the contact forces with the DOFs of the wheels, but unlike $\tilde{\mathbf{W}}_B(x)$, $\tilde{\mathbf{W}}_w$ does not depend on time. Superscript $()^{-\mathrm{T}}$ indicates the inverse of the transpose of the corresponding matrix. $\mathbf{r}_c(x)$ is the irregularities vector, consisting of the irregularities $r_c(x_i)$ at each contact point. We simulate the irregularities as stationary stochastic processes with the spectral representation method [26, 27].

Similarly, we obtain the EOM of the bridge from Equation (1) as:

$$\begin{aligned} &\mathbf{m}_B \ddot{\tilde{\mathbf{u}}}_B \\ &+ \left[\mathbf{c}_B + \tilde{\mathbf{W}}_B \mathbf{G}^{-1} \left(\tilde{\mathbf{W}}_w^{\mathrm{T}} \mathbf{m}_w^{-1} \mathbf{c}_w \tilde{\mathbf{W}}_w^{-\mathrm{T}} \tilde{\mathbf{W}}_B^{\mathrm{T}} - \tilde{\mathbf{W}}_B^{\mathrm{T}} \mathbf{m}_B^{-1} \mathbf{c}_B + 2v \tilde{\mathbf{W}}_B'^{\mathrm{T}} \right) \right] \dot{\tilde{\mathbf{u}}}_B \\ &+ \left[\mathbf{k}_B + \begin{pmatrix} \tilde{\mathbf{W}}_B \mathbf{G}^{-1} v \tilde{\mathbf{W}}_w^{\mathrm{T}} \mathbf{m}_w^{-1} \mathbf{c}_w \tilde{\mathbf{W}}_w^{-\mathrm{T}} \tilde{\mathbf{W}}_B'^{\mathrm{T}} + \tilde{\mathbf{W}}_w^{\mathrm{T}} \mathbf{m}_w^{-1} \mathbf{k}_w \tilde{\mathbf{W}}_w^{-\mathrm{T}} \tilde{\mathbf{W}}_B^{\mathrm{T}} \\ - \tilde{\mathbf{W}}_B^{\mathrm{T}} \mathbf{m}_B^{-1} \mathbf{k}_B + v^2 \tilde{\mathbf{W}}_B''^{\mathrm{T}} \end{pmatrix} \right] \tilde{\mathbf{u}}_B \\ &= \mathbf{f}_{B,\,\text{gravity}} - \tilde{\mathbf{W}}_B \mathbf{G}^{-1} \tilde{\mathbf{W}}_B^{\mathrm{T}} \mathbf{m}_B^{-1} \mathbf{f}_{B,\,\text{gravity}} \\ &- \mathbf{m}_B \boldsymbol{\delta}_B \ddot{\tilde{u}}_g + \tilde{\mathbf{W}}_B \mathbf{G}^{-1} \tilde{\mathbf{W}}_B^{\mathrm{T}} \boldsymbol{\delta}_B \ddot{\tilde{u}}_g - \tilde{\mathbf{W}}_B \mathbf{G}^{-1} \tilde{\mathbf{W}}_w^{\mathrm{T}} \boldsymbol{\delta}_w \ddot{\tilde{u}}_g \\ &- \tilde{\mathbf{W}}_B \mathbf{G}^{-1} \tilde{\mathbf{W}}_w^{\mathrm{T}} \mathbf{m}_w^{-1} \left[\mathbf{k}_w \tilde{\mathbf{W}}_w^{-\mathrm{T}} \mathbf{r}_c + v \mathbf{c}_w \tilde{\mathbf{W}}_w^{-\mathrm{T}} \mathbf{r}_c' + v^2 \mathbf{m}_w \tilde{\mathbf{W}}_w^{-\mathrm{T}} \mathbf{r}_c'' \right] \\ &- \tilde{\mathbf{W}}_B \mathbf{G}^{-1} \tilde{\mathbf{W}}_w^{\mathrm{T}} \mathbf{m}_w^{-1} \left(\mathbf{k}_{w,u} \tilde{\mathbf{u}}_u + \mathbf{c}_{w,u} \dot{\tilde{\mathbf{u}}}_u \right) \end{aligned} \tag{4}$$

where $\mathbf{f}_{B,\,\text{gravity}}$ denotes the self-weight of the vehicle acting on the bridge, and $\mathbf{G}^{-1}$ is the mass participating in the contact interaction between the wheels and the bridge and its inverse is $\mathbf{G}=\tilde{\mathbf{W}}^{\mathrm{T}}\mathbf{m}^{-1}\tilde{\mathbf{W}}$. Equations (3) and (4) represent the EOM of the upper part of the vehicle and bridge in a minimal manner (i.e., with the minimum number of DOFs [28]), as we eliminate the wheel part response from these equations [29].

In the previous study [22], we expressed the EOMs of both bridge (Equation (4)) and vehicle (Equation (3)) in dimensionless terms [30]. This dimensionless description enables to directly and consistently compare the order of magnitude of the various terms involved in the EOMs [22, 31]. This, in turn, allows us to identify negligible terms and, with the aid of an asymptotic expansion analysis technique about a small dimensionless parameter ε, to decouple the EOMs of the bridge and vehicle [22]. Typically, the frequency ratio $\Omega=\omega_p/\omega_B$ of the primary suspension system of the vehicle (ω_p) with respect to the fundamental frequency of the bridge (ω_B) is small (e.g., $O(\Omega)=10^{-1}$) [32, 33]. This allows to reformulate the original SVBI problem into a perturbation problem with respect to a small parameter $\varepsilon=\Omega$ [22]. In this study, we present the corresponding dimensional zero- and first-order EOMs of the bridge and vehicle resulting from the asymptotic expansion analysis to demonstrate the EMBS method. The zero-order in ε EOM of the bridge in dimensional form is:

$$\begin{gathered}\mathbf{m}_B\ddot{\tilde{\mathbf{u}}}_B^{(0)}+\left[\mathbf{c}_B+\tilde{\mathbf{W}}_B\mathbf{G}^{-1}\left(-\tilde{\mathbf{W}}_B^{\mathrm{T}}\mathbf{m}_B^{-1}\mathbf{c}_B+2v\tilde{\mathbf{W}}_B'^{\mathrm{T}}\right)\right]\dot{\tilde{\mathbf{u}}}_B^{(0)}+\left[\mathbf{k}_B-\tilde{\mathbf{W}}_B^{\mathrm{T}}\mathbf{m}_B^{-1}\mathbf{k}_B+v^2\tilde{\mathbf{W}}_B''^{\mathrm{T}}\right]\tilde{\mathbf{u}}_B^{(0)}\\ =\mathbf{f}_{B,\,\text{gravity}}-\tilde{\mathbf{W}}_B\mathbf{G}^{-1}\tilde{\mathbf{W}}_B^{\mathrm{T}}\mathbf{m}_B^{-1}\mathbf{f}_{B,\,\text{gravity}}\\ -\mathbf{m}_B\boldsymbol{\delta}_B\ddot{\tilde{u}}_g+\tilde{\mathbf{W}}_B\mathbf{G}^{-1}\tilde{\mathbf{W}}_B^{\mathrm{T}}\boldsymbol{\delta}_B\ddot{\tilde{u}}_g-\tilde{\mathbf{W}}_B\mathbf{G}^{-1}\tilde{\mathbf{W}}_w^{\mathrm{T}}\boldsymbol{\delta}_w\ddot{\tilde{u}}_g\\ -\tilde{\mathbf{W}}_B\mathbf{G}^{-1}\tilde{\mathbf{W}}_w^{\mathrm{T}}\mathbf{m}_w^{-1}\left[v^2\mathbf{m}_w\tilde{\mathbf{W}}_w^{-\mathrm{T}}\mathbf{r}_c''\right]\end{gathered} \tag{5}$$

where superscript $(\ )^{(0)}$ denotes the zero-order response. Similarly, the zero-order in ε response of the upper part of the vehicle results from:

$$\mathbf{m}_u\ddot{\tilde{\mathbf{u}}}_u^{(0)}+\mathbf{c}_u\dot{\tilde{\mathbf{u}}}_u^{(0)}+\mathbf{k}_u\tilde{\mathbf{u}}_u^{(0)}=-\mathbf{m}_u\boldsymbol{\delta}_u\ddot{\tilde{u}}_g\,. \tag{6}$$

Equations (5) and (6) indicate that the zero-order response of the bridge and vehicle depend solely on the properties of the bridge and vehicle, as well as on the irregularities and earthquake excitation, allowing for a decoupled analysis of the SVBI system.

We can obtain the first-order in ε response of the bridge $\left(\text{superscript}\,(\ )^{(1)}\right)$ by solving the following EOM:

$$\begin{gathered}\mathbf{m}_B\ddot{\tilde{\mathbf{u}}}_B^{(1)}+\left[\mathbf{c}_B+\tilde{\mathbf{W}}_B\mathbf{G}^{-1}\left(-\tilde{\mathbf{W}}_B^{\mathrm{T}}\mathbf{m}_B^{-1}\mathbf{c}_B+2v\tilde{\mathbf{W}}_B'^{\mathrm{T}}\right)\right]\dot{\tilde{\mathbf{u}}}_B^{(1)}+\left[\mathbf{k}_B-\tilde{\mathbf{W}}_B^{\mathrm{T}}\mathbf{m}_B^{-1}\mathbf{k}_B+v^2\tilde{\mathbf{W}}_B''^{\mathrm{T}}\right]\tilde{\mathbf{u}}_B^{(1)}\\ =-\tilde{\mathbf{W}}_B\mathbf{G}^{-1}\tilde{\mathbf{W}}_w^{\mathrm{T}}\mathbf{m}_w^{-1}\begin{pmatrix}v\mathbf{c}_w\tilde{\mathbf{W}}_w^{-\mathrm{T}}\mathbf{r}_c'\\ +\mathbf{c}_w\tilde{\mathbf{W}}_w^{-\mathrm{T}}\tilde{\mathbf{W}}_B^{\mathrm{T}}\dot{\tilde{\mathbf{u}}}_B^{(0)}+v\mathbf{c}_w\tilde{\mathbf{W}}_w^{-\mathrm{T}}\tilde{\mathbf{W}}_B'^{\mathrm{T}}\tilde{\mathbf{u}}_B^{(0)}\\ -\mathbf{k}_{w,u}\tilde{\mathbf{u}}_u^{(0)}-\mathbf{c}_{w,u}\dot{\tilde{\mathbf{u}}}_u^{(0)}\end{pmatrix}\,.\end{gathered} \tag{7}$$

The first-order EOM of the bridge (Equation (7)) depends on the zero-order response of both the bridge and vehicle, which we can derive from Equations (5) and (6). The combination of the zero- and first-order response yields an acceptable estimation of the bridge response, as demonstrated in [22]. Once we determine the bridge response, we can independently solve the EOM of the vehicle (Equation (3)) using the bridge response as input.

3 VEHICLE-BRIDGE SYSTEM DESCRIPTION

3.1 Bridge model: Alverca viaduct

The study focuses on the Alverca viaduct, a sophisticated railway bridge that integrates both track and substructure components, showcasing the effectiveness of the EMBS method in assessing large and intricate railway bridge systems. The Alverca viaduct is a flyover structure located on the northern line of the Portuguese railway network. It features several simply supported spans measuring 16.5 m, 17.5 m, and 21 m, supported by columns ranging in height from approximately 5 m to 15 m [34]. For simplicity, Montenegro et al. [24] standardized the span lengths and column heights across the structure, considering a total length of 630 m divided into 30 simply supported spans of 21 m each, all backed by columns of a uniform height of 10 m. This study adopts the model proposed by Montenegro et al. [24]. Figure 1 illustrates the examined bridge, including a perspective view (a), a cross-section view (b), and an elevation view (c).

The bridge deck comprises a prefabricated, prestressed U-shaped beam, with pre-slabs serving as formwork for the cast-in-situ concrete upper slab, resulting in a single-cell box girder deck. The deck is supported directly by elastomeric-reinforced bearings on the columns and abutments. Each span is fixed at one end and longitudinally guided at the other, while the transverse direction is fixed at both edges. The track in the existing viaduct consists of UIC60 rails with an Iberian gauge of 1.688 m, elastomeric rubber pads, prestressed concrete monoblock sleepers, and a 25 cm ballast layer beneath them. The columns have a rectangular solid cross-section with dimensions $2\times1\ \mathrm{m}^2$ (Figure 1(b)).

We develop the numerical model of the viaduct using ANSYS software [35]. We represent the deck, columns, sleepers, and rails with beam finite elements, while we model the bearing supports, ballast, and pads as linear spring-dampers. We employ mass point elements to simulate the ballast mass and non-structural elements, such as safety barriers and edge beams of the deck. We establish connections between the top of the columns and the deck, as well as between the deck and the track, using rigid frame elements. To ensure an accurate representation of the transition zones between the structure and the embankment, we model an extension of the track at both ends of the viaduct. Although the spans are disconnected from one another, the track provides a degree of transverse stiffness to the deck.

Following the approach of Montenegro et al. [24], the mechanical properties utilized in the numerical model of the deck are those reported in Malveiro et al. [34]. These properties are derived from a calibration process employing a genetic algorithm, which compares the modal parameters obtained from the numerical model with those from experimental tests. In this process, the track properties, specifically the ballast stiffness and the stiffness and damping of pads and fasteners, are sourced from the literature [24]. Table 1 presents the key mechanical properties of the numerical model of the viaduct [24]. Note that the study incorporates the effective stiffness of the piers to account for the reduction in the stiffness of the piers due to concrete cracking, in accordance with the procedure outlined by Montenegro et al. [24].

The mass and stiffness matrices of the bridge contain 156,168 DOFs after applying the support constraints. The vehicle is connected to the rail elements—referred to as target elements— through the bridge contact direction matrix $\tilde{\mathbf{W}}_B(x)$.

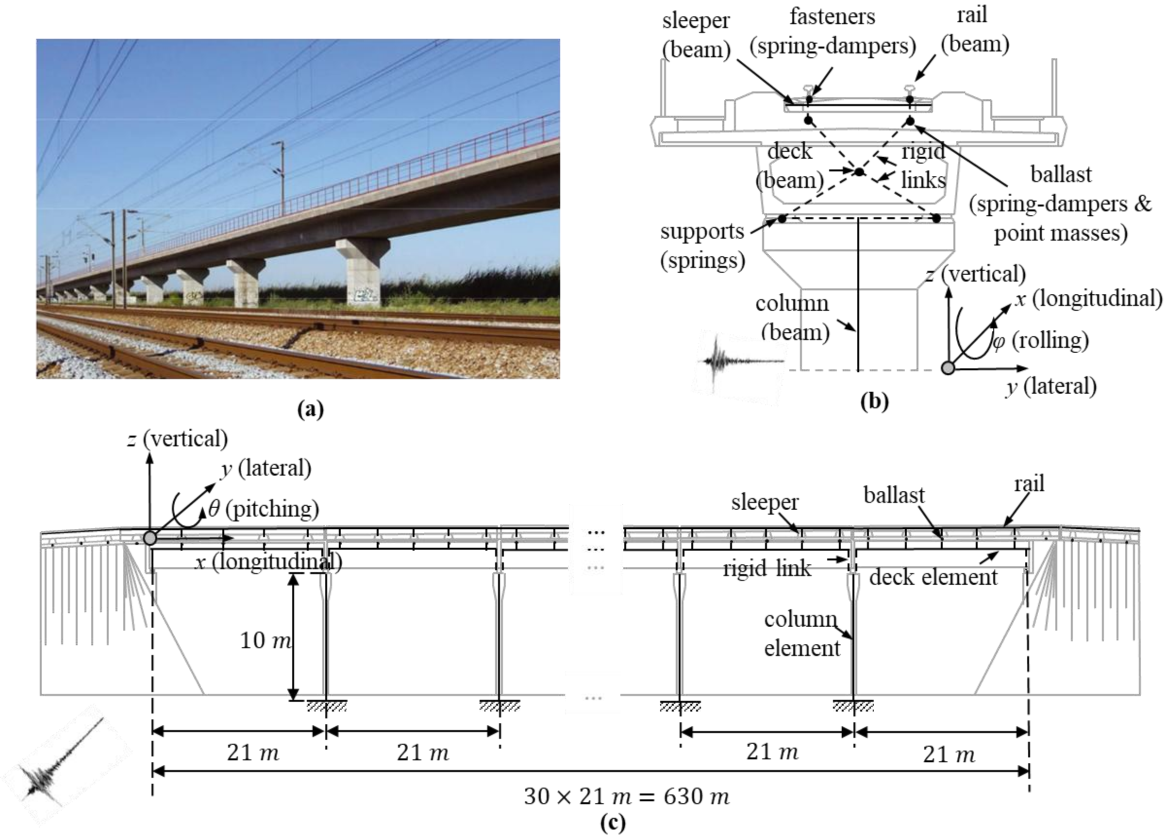

Figure 1: Alverca viaduct: (a) perspective view, (b) cross-section view, and (c) elevation view [24].

Table 1: Mechanical properties of the numerical model of the viaduct [24].

Parameter	Value
Modulus of elasticity of the upper slab concrete $E_{c,slab}$	33.48 GPa
Modulus of elasticity of the prefabricated beams concrete $E_{c,beam}$	48.08 GPa
Density of concrete ρ_c	2590.4 kg/m³
Modulus of elasticity of the sleepers concrete $E_{c,sleeper}$	40.90 GPa
Density of ballast ρ_{bal}	1995.9 kg/m³
Longitudinal stiffness of the ballast $K_{bal,l}$	30 MN/m/m
Transversal stiffness of ballast $K_{bal,t}$	7.5 MN/m/m
Vertical stiffness of ballast $K_{bal,v}$	100 MN/m/m
Damping of ballast (three directions) C_{bal}	50 kN·s/m/m
Longitudinal/transversal stiffness of fastener $K_{fas,l/t}$	20 MN/m
Vertical stiffness of fastener $K_{fas,v}$	500 MN/m
Rotational stiffness of fastener $K_{fas,r}$	45 kN·m/rad
Longitudinal/transversal damping of fastener $C_{fas,l/t}$	50 kN·s/m
Vertical damping of fastener $C_{fas,v}$	200 kN·s/m
Longitudinal stiffness of supports K_l	4.4 MN/m
Vertical stiffness of supports K_v	5200 MN/m

3.2 Train model

This study considers the Siemens Velaro AVE-S103 [25] (Spain, similar to the German ICE3) crossing the Alverca viaduct. We model the train as a 3D multibody assembly consisting of one car body (subscript $()_c$), two bogies (subscript $()_t$), and four wheelsets (subscript $()_w$) (see Figure 2). As we partition the DOFs of the vehicle into the "upper part" DOFs $\tilde{\mathbf{u}}_u(t)$, which are the DOFs not in contact with the bridge (subscript $()_u$), and the DOFs of the wheels, which are in contact with the bridge $\tilde{\mathbf{u}}_w(t)$ (subscript $()_w$) (Figure 2), the corresponding displacement vectors are:

$$\begin{aligned} \tilde{\mathbf{u}}_u^{\mathrm{T}} &= \left[\tilde{\mathbf{u}}_c^{\mathrm{T}} \quad \tilde{\mathbf{u}}_{t1}^{\mathrm{T}} \quad \tilde{\mathbf{u}}_{t2}^{\mathrm{T}} \right], \\ \tilde{\mathbf{u}}_w^{\mathrm{T}} &= \left[\tilde{\mathbf{u}}_{w1}^{\mathrm{T}} \quad \tilde{\mathbf{u}}_{w2}^{\mathrm{T}}\, \tilde{\mathbf{u}}_{w3}^{\mathrm{T}} \quad \tilde{\mathbf{u}}_{w4}^{\mathrm{T}} \right] \end{aligned} \tag{8}$$

with:

$$\begin{aligned} \tilde{\mathbf{u}}_c^{\mathrm{T}} &= \left[\tilde{y}_c \quad \tilde{z}_c \quad \tilde{\psi}_c \quad \tilde{\varphi}_c \quad \tilde{\theta}_c \right], \\ \tilde{\mathbf{u}}_{ti}^{\mathrm{T}} &= \left[\tilde{y}_{ti} \quad \tilde{z}_{ti} \quad \tilde{\psi}_{ti} \quad \tilde{\varphi}_{ti} \quad \tilde{\theta}_{ti} \right], \\ \tilde{\mathbf{u}}_{wj}^{\mathrm{T}} &= \left[\tilde{y}_{wj} \quad \tilde{z}_{wj} \quad \tilde{\varphi}_{wj} \right] \end{aligned} \tag{9}$$

where $i = 1,2$ denotes the number of bogies and $j = 1-4$ indicates the number of wheelsets. Thus, the train vehicle model has a total of 27 DOFs. In Equation (9) , $\tilde{y}$ and $\tilde{z}$ denote the transverse and vertical displacement; $\tilde{\psi}$, $\tilde{\varphi}$, and $\tilde{\theta}$ represent the yawing, rolling, and pitching rotations, respectively. Table 2 presents the mechanical and geometrical properties of the AVE-S103 high-speed train.

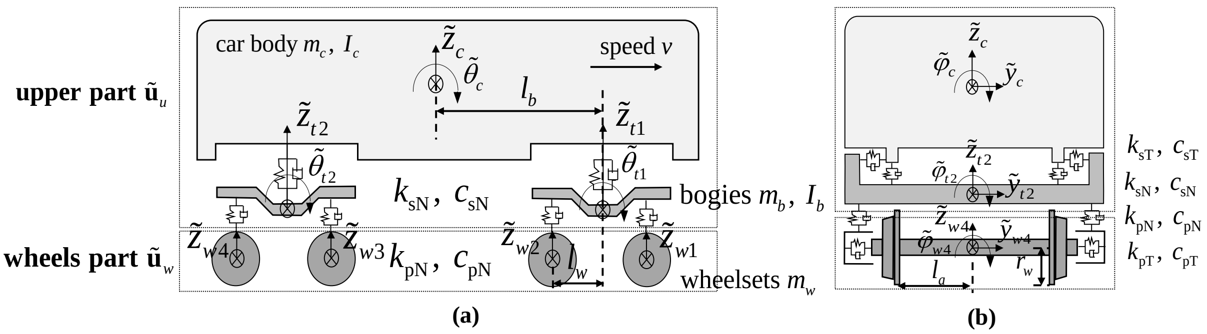

Figure 2: Train model: (a) longitudinal view and (b) transverse view [22].

Table 2: Mechanical and geometrical properties of the AVE-S103 high-speed train [25].

Parameter	**Value**
Car body mass m_{cb}	47800 kg
Car body roll moment of inertia $I_{cb,x}$	119328 kg·m^2
Car body pitch moment of inertia $I_{cb,y}$	1957888 kg·m^2
Car body yaw moment of inertia $I_{cb,z}$	1957888 kg·m^2
Bogie mass m_b	3500 kg
Bogie roll moment of inertia $I_{b,x}$	2835 kg·m^2
Bogie pitch moment of inertia $I_{b,y}$	1715 kg·m^2
Bogie yaw moment of inertia $I_{b,z}$	4235 kg·m^2
Wheelset mass m_w	1800 kg
Wheelset roll moment of inertia $I_{w,x}$	1000 kg·m^2
Wheelset yaw moment of inertia $I_{w,z}$	1000 kg·m^2
Stiffness of the primary longitudinal suspension $k_{1,x}$	12500 kN/m
Stiffness of the primary transversal suspension $k_{1,y}$	120000 kN/m
Stiffness of the primary vertical suspension $k_{1,z}$	1200 kN/m
Damping of the primary longitudinal suspension $c_{1,x}$	9 kN·s/m
Damping of the primary transversal suspension $c_{1,y}$	27.9 kN·s/m
Damping of the primary vertical suspension $c_{1,z}$	10 kN·s/m
Stiffness of the secondary longitudinal suspension $k_{2,x}$	240 kN/m
Stiffness of the secondary transversal suspension $k_{2,y}$	240 kN/m
Stiffness of the secondary vertical suspension $k_{2,z}$	350 kN/m
Damping of the secondary longitudinal suspension $c_{2,x}$	30 kN·s/m
Damping of the secondary transversal suspension $c_{2,y}$	30 kN·s/m
Damping of the secondary vertical suspension $c_{2,z}$	20 kN·s/m
Longitudinal distance between bogies d_b	17.375 m
Longitudinal distance between wheelsets d_w	2.50 m
Height of the carbody center of gravity h_{cb}	1.50 m
Height of the bogie center of gravity h_b	0.530 m
Nominal rolling radius R_0	0.43 m

4 NUMERICAL SIMULATIONS

In this section, we numerically simulate the vehicle-bridge system described in Section 3 and compare our results with those of Montenegro et al. [24]. Our proposed approach demonstrates some distinct differences compared to that of Montenegro et al. [24], which is expected to lead to minor differences in the obtained results. Montenegro et al. [24] utilized a wheel-rail contact model previously developed by the authors [36] and validated against experimental data. Additionally, Montenegro et al. [24] adopted a direct method to analyze [37].

For our numerical simulations, we consider a Siemens Velaro AVE-S103 train passing over the Alverca viaduct at a constant speed of 300 km/h during an earthquake excitation. We perform the VBI numerical simulations using MATLAB [38].

4.1 Earthquake excitation

In accordance with the approach of Montenegro et al. [24], this study assumes that the earthquake strikes solely in the lateral direction of the bridge. Figure 3 displays the ground motion acceleration history used for the numerical simulations [24].

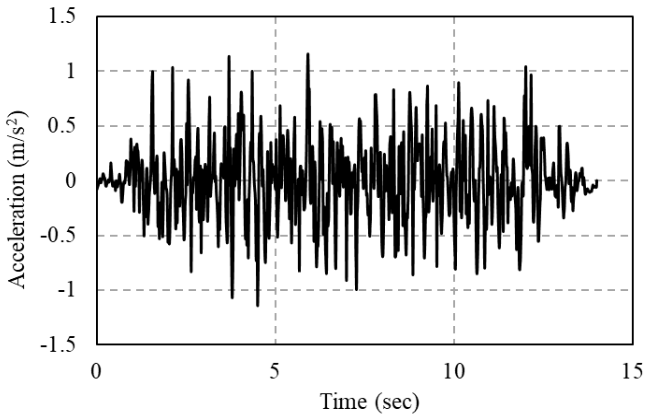

Figure 3: The ground motion acceleration history [24].

4.2 Numerical results

Figure 4 illustrates a comparison between the response histories of the Alverca viaduct and the Siemens Velaro AVE-S103 train, as obtained from the EMBS method and the study of Montenegro et al. [24]. Specifically, Figure 4 (a-d) displays the vertical and lateral displacement and acceleration at the mid-span of span 15 of the Alverca viaduct. Figure 4 (e and f) presents the lateral displacement and acceleration of the car body of the train while it traverses the viaduct. The results obtained from the EMBS method exhibit a good match with those obtained from the Montenegro et al. [24] method, as evident from the response history results (Figure 4). While some minor discrepancies are observed, they are deemed acceptable, considering that our proposed approach incorporates distinct differences from that of Montenegro et al. [24]. This overall similarity suggests that the EMBS method, which is a decoupled approach, yields results comparable to those obtained through the fully coupled solution method presented by Montenegro et al. [24].

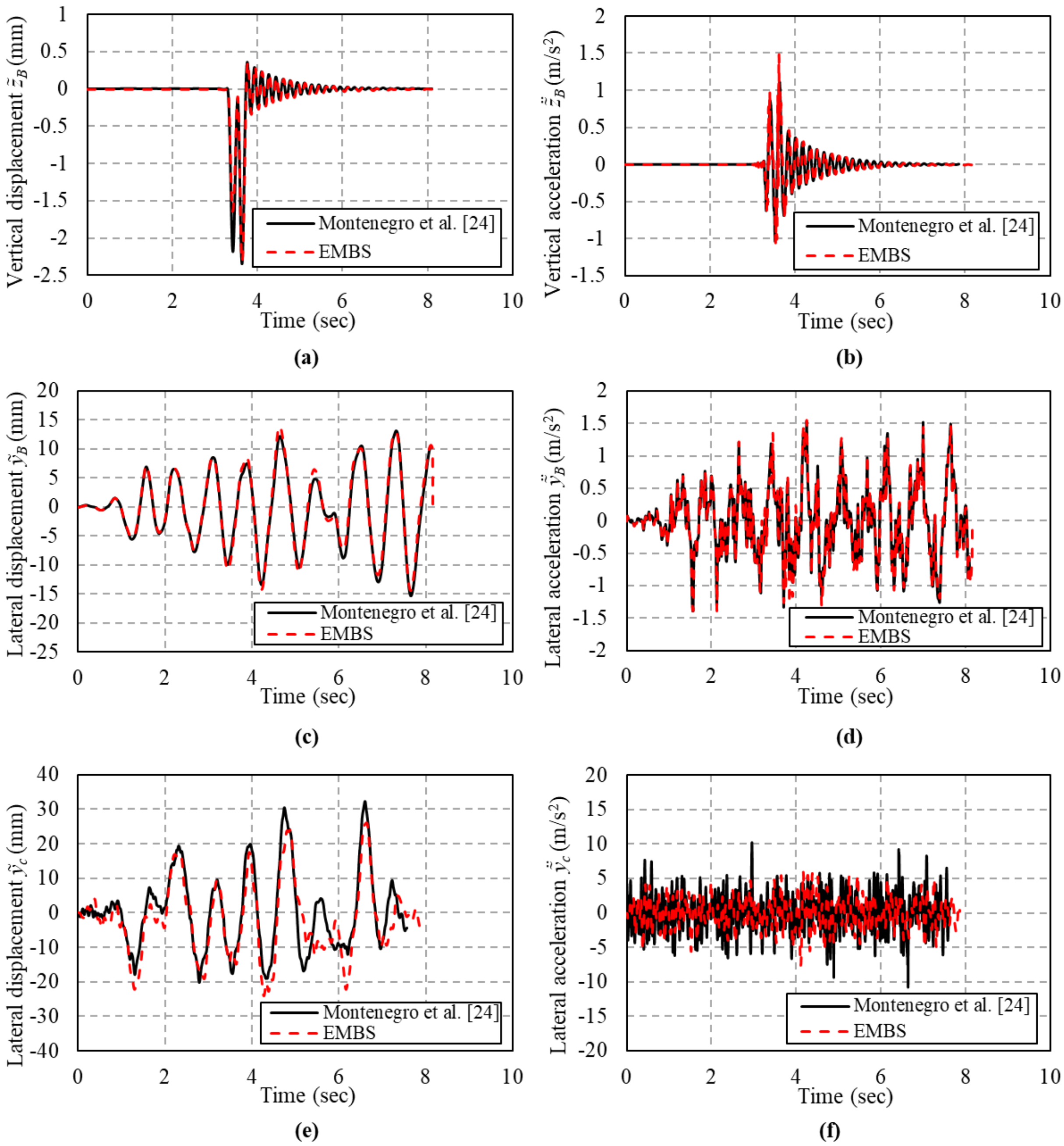

Figure 4: Response history of bridge and vehicle: (a) bridge vertical displacement, (b) bridge vertical acceleration, (c) bridge lateral displacement, (d) bridge lateral acceleration, (e) train car-body lateral displacement, and (f) train car-body lateral acceleration.

5 CONCLUSIONS

This study demonstrates the applicability of the established Extended Modified Bridge System (EMBS) method for analyzing a complex railway bridge. The EMBS method offers a consistent decoupling approach for vehicle-bridge interaction (VBI) analysis during earthquake excitation, eliminating the need to explicitly model the VBI in a coupled manner. The study outlines the EMBS formulation to provide a summary of the methodology. We examine the Alverca viaduct as a case study during the passage of a Siemens Velaro AVE-S103 train while an earthquake excitation strikes the bridge in the lateral direction. The results indicate that the EMBS method accurately returns the dynamics of a complex railway bridge system, considering also the track and substructure of the bridge, when compared to a coupled approach, such as that developed by Montenegro et al. [24]. This decoupled approach significantly simplifies the analysis of seismic vehicle-bridge interaction (SVBI).

6 ACKNOWLEDGEMENTS

The first and the fourth authors would like to acknowledge the support provided by the University Grants Committee Research Grants Council of Hong Kong, under Grant Reference Number GRF 16212522. The third author would like to acknowledge the Marie Skłodowska-Curie Actions (MSCA) Postdoctoral Fellow scheme under the OMORail project, Grand ID: 101104968.

REFERENCES

[1] H. Xia, N. Zhang, and W. Guo, *Dynamic interaction of train-bridge systems in high-speed railways*. Springer, 2018.

[2] X. He, T. Wu, Y. Zou, Y. F. Chen, H. Guo, and Z. Yu, “Recent developments of high-speed railway bridges in China,” *Struct. Infrastruct. Eng.*, vol. 13, no. 12, pp. 1584–1595, 2017, doi: 10.1080/15732479.2017.1304429.

[3] Z. Jin, W. Liu, S. Pei, and J. He, “Probabilistic assessment of vehicle derailment based on optimal ground motion intensity measure,” *Veh. Syst. Dyn.*, pp. 1–22, 2020, doi: 10.1080/00423114.2020.1792940.

[4] B. Wei, W. H. Wang, P. Wang, T. H. Yang, L. Z. Jiang, and T. Wang, “Seismic responses of a high-speed railway (HSR) bridge and track simulation under longitudinal earthquakes,” *J. Earthq. Eng.*, pp. 1–22, 2020, doi: 10.1080/13632469.2020.1832937.

[5] Q. Zeng and E. G. Dimitrakopoulos, “Seismic response analysis of an interacting curved bridge–train system under frequent earthquakes,” *Earthq. Eng. Struct. Dyn.*, vol. 45, no. 7, pp. 1129–1148, 2016, doi: 10.1002/eqe.2699.

[6] S. Kameshwar and J. E. Padgett, “Effect of vehicle bridge interaction on seismic response and fragility of bridges,” *Earthq. Eng. Struct. Dyn.*, vol. 47, no. 3, pp. 697–713, 2018, doi: 10.1002/eqe.2986.

[7] H. Homaei, E. G. Dimitrakopoulos, and A. Bakhshi, “Vehicle-bridge interaction and the tuned-mass damper effect on bridges during vertical earthquake excitation,” *Acta Mech.*, vol. 235, no. 3, pp. 1379–1394, 2024, doi: 10.1007/s00707-023-03533-2.

[8] H. Homaei and E. G. Dimitrakopoulos, “Does vehicle-bridge interaction resemble the effect of tuned-mass dampers on bridges during earthquakes?,” in *2nd Conference of the European Association on Quality Control of Bridges and Structures (EUROSTRUCT)*, 2023.

[9] Z. Jin, S. Pei, X. Li, H. Liu, and S. Qiang, “Effect of vertical ground motion on earthquake-induced derailment of railway vehicles over simply-supported bridges,” *J. Sound Vib.*, vol. 383, pp. 277–294, 2016, doi: 10.1016/j.jsv.2016.06.048.

[10] Q. Zeng and E. G. Dimitrakopoulos, “Vehicle–bridge interaction analysis modeling

derailment during earthquakes," *Nonlinear Dyn.*, vol. 93, no. 4, pp. 2315–2337, 2018, doi: 10.1007/s11071-018-4327-6.

[11] Y. B. Yang and Y. S. Wu, "Dynamic stability of trains moving over bridges shaken by earthquakes," *J. Sound Vib.*, vol. 258, no. 1, pp. 65–94, 2002, doi: 10.1006/jsvi.2002.5089.

[12] S. H. Ju, "Nonlinear analysis of high-speed trains moving on bridges during earthquakes," *Nonlinear Dyn.*, vol. 69, no. 1, pp. 173–183, 2012, doi: 10.1007/s11071-011-0254-5.

[13] Z. P. Zeng, Y. G. Zhao, W. T. Xu, Z. W. Yu, L. K. Chen, and P. Lou, "Random vibration analysis of train-bridge under track irregularities and traveling seismic waves using train-slab track-bridge interaction model," *J. Sound Vib.*, vol. 342, pp. 22–43, 2015, doi: 10.1016/j.jsv.2015.01.004.

[14] X. Liu, L. Jiang, P. Xiang, Y. Feng, Z. Lai, and X. Sun, "Evaluation of optimal ground motion intensity measures of high-speed railway train running safety on bridges during earthquakes," *Struct. Eng. Mech.*, vol. 81, no. 2, pp. 219–230, 2022, doi: 10.12989/sem.2022.81.2.219.

[15] W. Guo *et al.*, "Effect of near-fault vertical seismic excitation on running safety of trains on high-speed railway bridges," *Eng. Struct.*, vol. 296, 2023, doi: 10.1016/j.engstruct.2023.116880.

[16] H. W. Li, Z. D. Xu, D. Gomez, S. J. Dyke, Y. Q. Ni, and Y. W. Wang, "Seismic analysis of 3D train–wheel–bridge–bearing systems: Modeling," *Earthq. Eng. Struct. Dyn.*, vol. 52, no. 4, pp. 1205–1231, 2023, doi: 10.1002/eqe.3812.

[17] H. W. Li, Z. D. Xu, D. Gomez, S. J. Dyke, Y. W. Wang, and Y. Q. Ni, "Seismic analysis of 3D train–wheel–bridge–bearing systems: Illustrative examples," *Earthq. Eng. Struct. Dyn.*, vol. 52, no. 4, pp. 1252–1266, 2023, doi: 10.1002/eqe.3814.

[18] P. A. Montenegro *et al.*, "Assessment of train running safety on bridges: A literature review," *Eng. Struct.*, vol. 241, 2021, doi: 10.1016/j.engstruct.2021.112425.

[19] X. Luo, "Study on methodology for running safety assessment of trains in seismic design of railway structures," *Soil Dyn. Earthq. Eng.*, vol. 25, no. 2, pp. 79–91, 2005, doi: 10.1016/j.soildyn.2004.10.005.

[20] Z. Jin, W. Liu, and S. Pei, "A code-type method to assess the running safety of railway vehicles on bridges shaken by earthquakes including girder's torsional motion," *Int. J. Struct. Stab. Dyn.*, 2022, doi: 10.1142/S0219455423500013.

[21] Z. Zhu, W. Gong, G. Zhou, Y. Yang, and L. Jiang, "A simplified weak coupling dynamic analysis method for running safety evaluation of train on bridges under earthquake excitation," *Eng. Struct.*, vol. 309, p. 118072, 2024, doi: 10.1016/j.engstruct.2024.118072.

[22] H. Homaei, C. D. Stoura, and E. G. Dimitrakopoulos, "Extended Modified Bridge System (EMBS) method for decoupling seismic vehicle-bridge interaction," *Earthq. Eng. Struct. Dyn.*, vol. 53, no. 13, pp. 4054–4075, 2024, doi: 10.1002/eqe.4209.

[23] C. D. Stoura and E. G. Dimitrakopoulos, "MDOF extension of the Modified Bridge System method for vehicle–bridge interaction," *Nonlinear Dyn.*, vol. 102, no. 4, pp. 2103–2123, 2020, doi: 10.1007/s11071-020-06022-6.

[24] P. A. Montenegro, R. Calçada, N. Vila Pouca, and M. Tanabe, "Running safety assessment of trains moving over bridges subjected to moderate earthquakes," *Earthq. Eng. Struct. Dyn.*, vol. 45, no. 3, pp. 483–504, 2016, doi: 10.1002/eqe.2673.

[25] P. A. Montenegro *et al.*, "Impact of the train-track-bridge system characteristics in the runnability of high-speed trains against crosswinds - Part I: Running safety," *J. Wind Eng. Ind. Aerodyn.*, vol. 224, 2022, doi: 10.1016/j.jweia.2022.104974.

[26] E. G. Dimitrakopoulos and Q. Zeng, "A three-dimensional dynamic analysis scheme for the interaction between trains and curved railway bridges," *Comput. Struct.*, vol. 149, no. 1, pp. 43–60, 2015, doi: 10.1016/j.compstruc.2014.12.002.

[27] Y. B. Yang, J. D. Yau, and Y. S. Wu, *Vehicle–Bridge Interaction Dynamics: With Applications to High-Speed Railways*. 2004. doi: 10.1142/5541.

[28] E. Paraskevopoulos and S. Natsiavas, "On application of Newton's law to mechanical systems with motion constraints," *Nonlinear Dyn.*, vol. 72, pp. 455–475, 2013, doi: 10.1007/s11071-012-0727-1.

[29] C. D. Stoura, E. Paraskevopoulos, E. G. Dimitrakopoulos, and S. Natsiavas, "A Dynamic Partitioning Method to solve the vehicle-bridge interaction problem," *Comput. Struct.*, vol. 251, p. 106547, 2021, doi: 10.1016/j.compstruc.2021.106547.

[30] H. Homaei and E. G. Dimitrakopoulos, "Extended modified bridge system method for vehicle-bridge interaction: treatment of rotational degrees of freedom," in *9th International Conference on Computational Methods in Structural Dynamics and Earthquake Engineering (COMPDYN)*, 2023.

[31] H. Homaei, C. D. Stoura, and E. G. Dimitrakopoulos, "A rational approach for decoupling the vehicle-bridge interaction problem under the effect of earthquake excitation," in *18th World Conference on Earthquake Engineering (WCEE)*, 2024.

[32] *ERRI, Rail bridges for speeds>200 km/h- Final report*. in ERRI D 214/RP9. Utrecht: European Rail Research Institute, 1999.

[33] "European Committee for Standardization (CEN): Eurocode 1: Actions on structures-Part 2: Traffic loads on bridges.," 2003.

[34] J. Malveiro, D. Ribeiro, R. Calçada, and R. Delgado, "Updating and validation of the dynamic model of a railway viaduct with precast deck," *Struct. Infrastruct. Eng.*, vol. 10, no. 11, pp. 1484–1509, 2014, doi: 10.1080/15732479.2013.833950.

[35] "ANSYS®. Academic Research, Release 2024 R1, ANSYS Inc."

[36] P. A. Montenegro, S. G. M. Neves, R. Calçada, M. Tanabe, and M. Sogabe, "Wheel-rail contact formulation for analyzing the lateral train-structure dynamic interaction," *Comput. Struct.*, vol. 152, pp. 200–214, 2015, doi: 10.1016/j.compstruc.2015.01.004.

[37] S. G. M. Neves, P. A. Montenegro, A. F. M. Azevedo, and R. Calçada, "A direct method for analyzing the nonlinear vehicle–structure interaction," *Eng. Struct.*, vol. 69, pp. 83–89, doi: 10.1016/j.engstruct.2014.02.027.

[38] "MATLAB®. Release R2024a, The MathWorks Inc., Natick, MA, USA; 2024."